Stephen C. Warren-Smith, Roman Kostecki, Linh Viet Nguyen, and Tanya M. Monro
Fabrication, splicing, Bragg grating writing, and polyelectrolyte functionalization of exposed-core microstructured optical fibers
Optics Express, 2014; 22(24):29493-29504

Fabrication, splicing, Bragg grating writing, and polyelectrolyte functionalization of exposed-core microstructured optical fibers

Stephen C. Warren-Smith*, Roman Kostecki, Linh Viet Nguyen, and Tanya M. Monro

Institute for Photonics and Advanced Sensing (IPAS) and ARC Centre of Excellence in Nanoscale BioPhotonics, The University of Adelaide, Adelaide 5005, Australia

*stephen.warrensmith@adelaide.edu.au

Abstract: Femtosecond laser written Bragg gratings have been written in exposed-core microstructured optical fibers with core diameters ranging from 2.7 µm to 12.5 µm and can be spliced to conventional single mode fiber. Writing a Bragg grating on an open core fiber allows for real-time refractive index based sensing, with a view to multiplexed biosensing. Smaller core fibers are shown both experimentally and theoretically to provide a higher sensitivity. A 7.5 µm core diameter fiber is shown to provide a good compromise between sensitivity and practicality and was used for monitoring the deposition of polyelectrolyte layers, an important first step in developing a biosensor.

OCIS codes: (060.2280) Fiber design and fabrication; (060.2370) Fiber optics sensors; (060.3735) Fiber Bragg gratings; (060.4005) Microstructured fibers.

References and links

1. T. A. Birks, J. C. Knight, and P. S. J. Russell, "Endlessly single-mode photonic crystal fiber," Opt. Lett. **22**, 961-963 (1997).
2. R. F. Cregan, B. J. Mangan, J. C. Knight, T. A. Birks, P. S. J. Russell, P. J. Roberts, and D. C. Allan, "Single-mode photonic band gap guidance of light in air," Science **285**, 1537-1539 (1999).
3. W. J. Wadsworth, R. M. Percival, G. Bouwmans, J. C. Knight, T. A. Birks, T. D. Hedley, and P. S. J. Russel, "Very high numerical aperture fibers," IEEE Photonic. Tech. L. **16**, 843-845 (2004).
4. K. Furusawa, A. Malinowshi, J. H. V. Price, T. M. Monro, J. K. Sahu, J. Nilsson, and D. J. Richardson, "Cladding pumped ytterbium-doped fiber laser with holey inner and outer cladding," Opt. Express **9**, 714-720 (2001).
5. J. K. Sahu, C. C. Renaud, K. Furusawa, R. Selvas, J. A. Alvarez-Chavez, D. J. Richardson, and J. Nilsson, "Jacketed air-clad cladding pumped ytterbium-doped fibre laser with wide tuning range," Electron. Lett. **37**, 1116-1117 (2001).
6. J. Laegsgaard and A. Bjarklev, "Microstructured optical fibers-fundamentals and applications," J. Am. Ceram. Soc. **89**, 2-12 (2006).
7. A. S. Webb, F. Poletti, D. J. Richardson, and J. K. Sahu, "Suspended-core holey fiber for evanescent-field sensing," Opt. Eng. **46**, 10503 (2007).
8. X. Feng, A. K. Mairaj, D. W. Hewak, and T. M. Monro, "Nonsilica glasses for holey fibers," J. Lightwave Technol. **23**, 2046-2054 (2005).
9. H. Ebendorff-Heidepriem and T. M. Monro, "Extrusion of complex preforms for microstructured optical fibers," Opt. Express **15**, 15086-15092 (2007).
10. H. Ebendorff-Heidepriem, S. C. Warren-Smith, and T. M. Monro, "Suspended nanowires: Fabrication, design and characterization of fibers with nanoscale cores," Opt. Express **17**, 2646-2657 (2009).
11. S. C. Warren-Smith, H. Ebendorff-Heidepriem, T. C. Foo, R. Moore, C. Davis, and T. M. Monro, "Exposed-core microstructured optical fibers for real-time fluorescence sensing," Opt. Express **17**, 18533-18542 (2009).
12. S. Atakaramians, S. Afshar V., H. Ebendorff-Heidepriem, M. Nagel, B. M. Fischer, D. Abbott, and T. M. Monro, "THz porous fibers: design, fabrication and experimental characterization," Opt. Express **17**, 14053-14062 (2009).
13. T. M. Monro, S. C. Warren-Smith, E. P. Schartner, A. Francois, S. Heng, H. Ebendorff-Heidepriem, and S. Afshar V, "Sensing with suspended-core optical fibers," Opt. Fiber Technol. **16**, 343-356 (2010).
14. T. M. Monro, D. J. Richardson, and P. J. Bennett, "Developing holey fibres for evanescent field devices," Electron. Lett. **35**, 1188-1189 (1999).

15. Y. Zhu, R. T. Bise, J. Kanka, P. Peterka, and H. Du, "Fabrication and characterization of solid-core photonic crystal fiber with steering-wheel air-cladding for strong evanescent field overlap," Opt. Commun. **281**, 55-60 (2008).
16. Y. Zhu, H. Du, and R. Bise, "Design of solid-core microstructured optical fiber with steering-wheel air cladding for optimal evanescent-field sensing," Opt. Express **14**, 3541-3546 (2006).
17. J. B. Jensen, L. H. Pedersen, P. E. Hoiby, L. B. Nielsen, T. P. Hansen, J. R. Folkenberg, J. Riishede, D. Noordegraaf, K. Nielsen, A. Carlsen, and A. Bjarklev, "Photonic crystal fiber based evanescent-wave sensor for detection of biomolecules in aqueous solutions," Opt. Lett. **29**, 1974-1976 (2004).
18. S. Afshar V, S. C. Warren-Smith, and T. M. Monro, "Enhancement of fluorescence-based sensing using microstructured optical fibres," Opt. Express **15**, 17891-17901 (2007).
19. T. Ritari, J. Tuominen, H. Ludvigsen, J. C. Petersen, T. Sorensen, T. P. Hansen, and H. R. Simonsen, "Gas sensing using air-guiding photonic bandgap fibers," Opt. Express **12**, 4080-4087 (2004).
20. C. J. Hensley, D. H. Broaddus, C. B. Schaffer, and A. L. Gaeta, "Photonic band-gap fiber gas cell fabricated using femtosecond micromachining," Opt. Express **15**, 6690-6695 (2007).
21. O. Frazao, J. L. Santos, F. M. Araujo, and L. A. Ferreira, "Optical sensing with photonic crystal fibers," Laser and Photonic Reviews **2**, 449-459 (2008).
22. S. C. Warren-Smith, S. Heng, H. Ebendorff-Heidepriem, A. D. Abell, and T. M. Monro, "Fluorescence-based aluminum ion sensing using a surface functionalized microstructured optical fiber," Langmuir **27**, 5680-5685 (2011).
23. S. Heng, A. M. Mak, D. B. Stubing, T. M. Monro, and A. D. Abell, "A dual sensor for Cd(II) and Ca(II): selective nanoliter-scale sensing of metal ions," Anal. Chem. **86**, 3268-3272 (2014).
24. L. Rindorf, P. E. Hoiby, J. B. Jensen, L. H. Pedersen, O. Bang, and O. Geschke, "Towards biochips using microstructured optical fiber sensors," Anal. Bioanal. Chem. **385**, 1370-1375 (2006).
25. Y. Ruan, T. C. Foo, S. Warren-Smith, P. Hoffmann, R. C. Moore, H. Ebendorff-Heidepriem, and T. M. Monro, "Antibody immobilization within glass microstructured fibers: a route to sensitive and selective biosensors," Opt. Express **16**, 18514-18523 (2008).
26. J. B. Jensen, P. E. Hoiby, G. Emiliyanov, O. Bang, L. H. Pedersen, and A. Bjarklev, "Selective detection of antibodies in microstructured polymer optical fibers," Opt. Express **13**, 5883-5889 (2005).
27. G. Emiliyanov, J. B. Jensen, O. Bang, P. E. Hoiby, L. H. Pedersen, E. M. Kjaer, and L. Lindvold, "Localized biosensing with Topas microstructured polymer optical fiber," Opt. Lett. **32**, 460-462 (2007).
28. M. Hautakorpi, M. Mattinen, and H. Ludvigsen, "Surface-plasmon-resonance sensor based on three-hole microstructured optical fiber," Opt. Express **16**, 8427-8432 (2008).
29. A. Wang, A. Docherty, B. T. Kuhlmey, F. M. Cox, and M. C. J. Large, "Side-hole fiber sensor based on surface plasmon resonance," Opt. Lett. **34**, 3890-3892 (2009).
30. A. Hassani and M. Skorobogatiy, "Design of the microstructured optical fiber-based surface plasmon resonance sensors with enhanced microfluidics," Opt. Express **14**, 11616-11621 (2006).
31. B. Gauvreau, A. Hassani, M. F. Fehri, A. Kabashin, and M. A. Skorobogatiy, "Photonic bandgap fiber-based surface plasmon resonance sensors," Opt. Express **15**, 11413-11426 (2007).
32. G. Emiliyanov, P. E. Hoiby, L. H. Pedersen, and O. Bang, "Selective serial multi-antibody biosensing with TOPAS microstructured polymer optical fibers," Sensors **13**, 3242-3251 (2013).
33. B. Culshaw, "Optical fiber sensor technologies: opportunities and-perhaps-pitfalls," J. Lightwave Technol. **22**, 39-50 (2004).
34. Y. Liu, C. Meng, P. Zhang, Y. Xiao, H. Yu, and L. Tong, "Compact microfiber Bragg gratings with high-index contrast," Opt. Lett. **36**, 3115-3117 (2011).
35. A. Iadicicco, A. Cusano, A. Cutolo, R. Bernini, and M. Giordano, "Thinned fiber Bragg gratings as high sensitivity refractive index sensor," IEEE Photonic. Tech. L. **16**, 1149-1151 (2004).
36. W. Liang, Y. Huang, Y. Xu, R. K. Lee, and A. Yariv, "Highly sensitive fiber Bragg grating refractive index sensors," Appl. Phys. Lett. **86**, 151122 (2005).
37. B. N. Shivananju, M. Renilkumar, G. R. Prashanth, S. Asokan, and M. M. Varma, "Detection limit of etched fiber Bragg grating sensors," J. Lightwave Technol. **31**, 2441-2447 (2013).
38. M. C. P. L. Huy, G., V. Dewynter, P. Ferdinand, P. Roy, J.-L. Auguste, D. Pagnoux, W. Blanc, and B. Dussardier, "Three-hole microstructured optical fiber for efficient fiber Bragg grating refractometer," Opt. Lett. **32**, 2390-2392 (2007).
39. A. Candiani, A. Bertucci, S. Giannetti, M. Konstantaki, A. Manicardi, S. Pissadakis, A. Cucinotta, R. Corradini, and S. Selleri, "Label-free DNA biosensor based on a peptide nucleic acid-functionalized microstructured optical fiber-Bragg grating," J. Biomed. Opt. **18**, 057004-057001-057006 (2013).
40. S. C. Warren-Smith and T. M. Monro, "Exposed core microstructured optical fiber Bragg gratings: refractive index sensing," Opt. Express **22**, 1480-1489 (2014).
41. R. Kostecki, H. Ebendorff-Heidepriem, S. C. Warren-Smith, and T. M. Monro, "Predicting the drawing conditions for microstructured optical fiber fabrication," Opt. Mater. Express **4**, 29-40 (2014).
42. R. Kostecki, H. Ebendorff-Heidepriem, C. Davis, G. McAdam, S. C. Warren-Smith, and T. M. Monro, "Silica exposed-core microstructured optical fibers," Opt. Mater. Express **2**, 1538-1547 (2012).
43. R. Kostecki, H. Ebendorff-Heidepriem, S. Afshar V., G. McAdam, C. Davis, and T. M. Monro, "Novel polymer functionalization method for exposed-core optical fiber," Opt. Mater. Express **4**, 1515-1525 (2014).

44. G. Tsiminis, F. Chu, S. C. Warren-Smith, N. A. Spooner, and T. M. Monro, "Identification and quantification of explosives in nanolitre solution volumes by Raman spectroscopy in suspended core optical fibers " Sensors **13**, 13163-13177 (2013).
45. K. Okamoto, *Fundamentals of Optical Waveguides* (Academic, 2000).
46. J. Wooler, S. R. Sandoghchi, D. Gray, F. Poletti, M. N. Petrovich, N. V. Wheeler, N. K. Baddela, and D. Richardson, "Overcoming the challenges of splicing dissimilar diameter solid-core and hollow-core photonic band gap fibers," Workshop on Specialty Optical Fibers and their Applications (2013).
47. L. Xiao, W. Jin, and M. S. Demokan, "Fusion splicing small-core photonic crystal fibers and single-mode fibers by repeated arc discharges," Opt. Lett. **31**, 115-117 (2007).
48. L. Xiao, M. S. Demokan, W. Jin, Y. Wang, and C.-L. Zhao, "Fusion splicing photonic crystal fibers and conventional single-mode fibers: microhole collapse effect," J. Lightwave Technol. **25**, 2563-2574 (2007).
49. G. V. Steenberge, P. Geerinck, S. V. Put, J. Watte, H. Ottevaere, H. Thienpont, and P. V. Daele, "Laser cleaving of glass fibers and glass fiber arrays," J. Lightwave Technol. **23**, 609-614 (2005).
50. K.-Y. Chu and A. R. Thompson, "Densities and refractive indices of alcohol-water solutions," J. Chem. Eng. Data **7**, 358-360 (1962).
51. Y. Zhang, H. Shibru, K. L. Cooper, and A. Wang, "Miniature fiber-optic multicavity Fabry-Perot interferometric biosensor," Opt. Lett. **30**, 1021-1023 (2005).
52. D. W. Kim, Y. Zhang, K. L. Cooper, and A. Wang, "Fibre-optic interferometric immuno-sensor using long period grating," Electron. Lett. **42**, 324-325 (2006).

1. Introduction

The advent of microstructured optical fibers (MOFs) has provided significant freedom in designing the optical and physical properties of optical fibers. Fibers can now be fabricated with features such as endlessly single mode guidance [1], air-guiding via the photonic bandgap effect [2], and high numerical aperture double clad structures for fiber lasers [3-5]. To achieve such structures numerous techniques have been developed such as capillary stacking [6], drilling [7, 8], and extrusion [9, 10]. Each technique has its own advantages, for example, capillary stacking can be used to create highly regular periodic structures, drilling can be used to form arbitrarily located circular features, while extrusion has the capacity to form non-circular features [11, 12]. Of particular interest here is the sensing ability of MOFs. It is well known that a portion of the guided modes can propagate within the holes of the fiber. This can be a significant fraction of the guided modes in the case of index-guiding solid-core structures, if the core diameter is sufficiently small [13-18]. Alternatively, close to 100% of the light can propagate within the air-core of photonic bandgap structures [19-21].

MOF sensors have gained particular attention in the literature for absorption and fluorescence based chemical and biological sensing. For example, gas sensing can be achieved by directly measuring the spectral features of an analyte that has been loaded into the MOF holes. For the measurement of chemical species without strong or distinguishable spectral features in the transmission window of silica glass it is common to make use of transduction molecules that provide a fluorescence enhancement (or quenching) upon binding with the target analyte. This has been demonstrated for species including aluminum ions [22], and cadmium and calcium ions [23]. Similarly, MOF biosensors can make use of either absorption [17, 24], fluorescence-based labelling techniques [25-27], or surface plasmon resonance for refractive-index based label free detection [28-31]. Unfortunately, the above methods of biosensing all suffer from negating one of the greatest strengths of the optical fiber sensing, which is the ability to perform significant wavelength division multiplexed measurements. While there are occasional examples of measuring two biomolecules [32], the broadband nature of fluorescence and surface plasmon resonance makes it prohibitive to perform the type of multiplexed assays routinely required in the life sciences.

Fiber Bragg gratings (FBGs) offer a straightforward approach to multiplexed sensing, and they are now used routinely to provide multiplexed temperature and strain measurements [33]. Due to their narrow bandwidth it is possible to perform significantly greater multiplexing than can be achieved on a single fiber with either surface plasmon resonance or fluorescence based biosensing. Refractive-index based sensing using Bragg gratings has focused on the use of

micro/nano-fibers (e.g. tapered or etched optical fibers) [34-37] and, to a lesser extent, microstructured optical fiber Bragg gratings [38, 39]. Part of the challenge in such work is to create a Bragg grating that is highly sensitive to changes outside the fiber core, which generally involves reducing the core diameter, while also allowing for: easy interaction with a liquid analyte, access to the core for Bragg grating inscription, integration with commercial interrogation equipment, and physical robustness for real-world applications.

In this work we advance the ability to use a new class of optical fiber, termed the exposed-core microstructured optical fiber (EC-MOF), by demonstrating how they can be inscribed with Bragg gratings for biosensing applications. Compared to an unclad micro/nano-fiber, this class of fiber provides the physical robustness of a standard fiber, while allowing a portion of the small, sensitive core to be externally accessible along its length for both Bragg grating inscription and ease of interacting with external analytes. Previously, we have reported the fabrication of Bragg gratings in a large core (12.5 μm) EC-MOF, which yielded a modest sensitivity averaging 1.7 nm/RIU over the refractive index range of 1.333 (water) to 1.377 (isopropanol) [40].

Here we investigate the fabrication, splicing, and Bragg grating inscription of smaller core EC-MOFs and demonstrate both experimentally and theoretically that smaller core fibers yield significantly higher sensitivity to changes in refractive index. In particular, we demonstrate experimentally a four-fold increase in sensitivity by using a 7.5 μm core diameter EC-MOF and a sixty-fold increase for a 2.7 μm core diameter fiber. The intermediate core size provides a good compromise between sensitivity and ease of use (e.g. splicing), and is demonstrated to be sufficiently sensitive to measure polyelectrolyte deposition, an important first step in developing a label-free biosensor.

2. Cross-sectional structure: fiber fabrication

The fabrication of microstructured optical fibers is generally a two-step technique [6]. First a preform is fabricated that has a macroscopic structure that closely resembles the desired fiber geometry. Some deformation of the structure will occur during fiber drawing depending on the draw parameters and effects related to surface tension and material viscosity. Secondly, the preform is drawn into fiber using a draw tower, where control of parameters such as temperature, internal pressurization, and feed and draw speeds allow some degree of fine-tuning of the final geometry. In some cases it is necessary to introduce an additional step where the preform is canned and then sleeved before finally drawing into fiber. This can allow for a reduction in size of the final features of the fiber, such as enabling the production of sub-micron core sizes [10].

2.1 Fiber preform

In this work we have used ultrasonic drilling and milling or cutting to prepare the preform. While the details of this fabrication process have been detailed elsewhere [41, 42], here we show the versatility of this technique to develop a range of different structures. The preforms were fabricated by first ultrasonic drilling three holes (2.8 mm in this work) into either 12 mm or 20 mm F300HQ (Heraeus) silica rods in an equilateral triangle pattern [Fig. 1]. This can either be done centrally in the preform [Figs. 1(a) and 1(c)] or offset from the center [Fig. 1(b)]. To create an exposed-core, the preform can either be milled [Fig. 1(b)] or cut with a diamond blade [Fig. 1(c)].

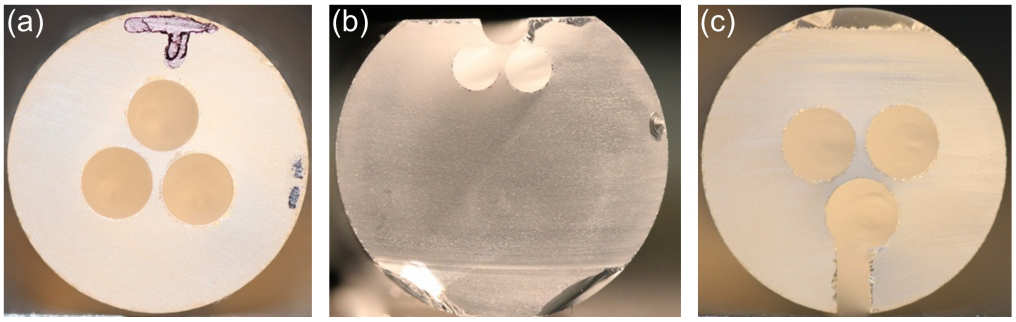

Fig. 1. Preforms demonstrating the various structures that can be utilized for exposed-core fiber fabrication. (a) Drilling, (b) milling, and (c) cutting. The diameter of the preforms are (a) 12 mm, (b) 12 mm, and (c) 20 mm.

2.2 Fiber drawing

The preforms were drawn into fiber using a 6 m tall drawing tower with a graphite resistance furnace and positive internal pressure. Detailed drawing conditions for the fibers in Figs. 2(a) and 2(d) can be found in [42] and [41], respectively. For both fibers in Figs. 2(b) and 2(c) the conditions used were: a draw temperature of 1976^{o}C, a preform feed rate of 1.0 mm/min, and an internal pressure of 1100 Pa. Four different designs of EC-MOF were fabricated [Fig. 2] with different core diameters (12.5 µm, 7.5 µm, 9.3 µm, and 2.7 µm) and varying core accessibility. That is, the open wedge that exposes the core varies from open [Figs. 2(a) and 2(b)] to a more closed form [Figs. 2(c) and 2(d)].

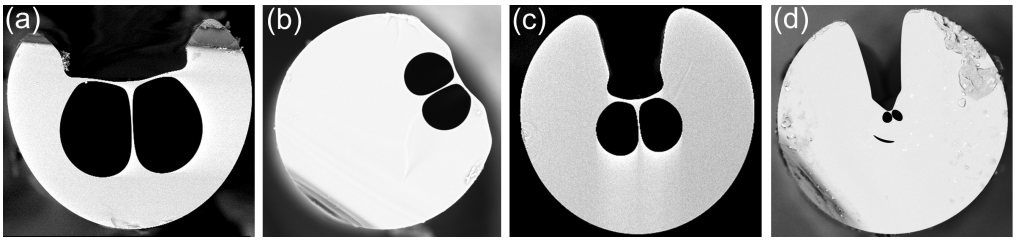

Fig. 2. Scanning electron images (SEMs) of the EC-MOFs that have been fabricated. The fibers have effective core diameters of (a) 12.5 µm [42], (b) 9.3 µm, (c) 7.5 µm [43], and (d) 2.7 µm [41]. The outer diameters at the maximum point of the fibers are (a) 200 µm, (b) 200 µm, (c) 160 µm, and (d) 200 µm.

2.3 Splicing to conventional single mode fiber: theory

One of the most important practical considerations when using EC-MOFs is the ability to splice such fibers to conventional single mode fiber (SMF). This both improves the coupling stability into the EC-MOF and allows for easier integration with commercial interrogation equipment.

One of the first considerations is matching the mode size (e.g. mode field diameter) of the single mode fiber with the EC-MOF. Thus, we have calculated the splice loss when coupling from the SMF into the fundamental mode of the EC-MOFs. Note that the EC-MOFs are multimode and thus the total coupling efficiency can be greater than that calculated here. Depending on the application, coupling into higher order modes may, or may not, be desirable and could be considered in future work. For the purposes of Bragg grating based sensing, we have observed experimentally that coupling into the fundamental mode provides the most stable signal as the Bragg grating peak associated with the fundamental mode is spectrally isolated from reflections associated with higher order modes, which tend to overlap each other.

The splice loss has been calculated using Eq. (1) [44].

$$\alpha_{SL} = -10\log_{10}\left[\left|\frac{2(\int_{\infty}\vec{e}_S\times\vec{h}_E\cdot\vec{z}dA)(\int_{\infty}\vec{e}_E\times\vec{h}_S\cdot\vec{z}dA)}{\int_{\infty}\vec{e}_S\times\vec{h}_E\cdot\vec{z}dA+\int_{\infty}\vec{e}_E\times\vec{h}_S\cdot\vec{z}dA}\right|^2\right] \quad (1)$$

In Eq. (1), $\vec{e}$ and $\vec{h}$ are the electric and magnetic fields of the fundamental modes of the single-mode (S) and exposed-core (E) fibers, respectively, α_{SL} is the splice loss (in dB), and $\vec{z}$ is a unit vector along the fiber axis.

The electric and magnetic modes have been calculated using an analytic model for the step-index fiber [45] and the modes of the EC-MOFs where calculated by importing SEM images into COMSOL v3.4, as has been done previously for the EC-MOF in Fig. 2(a) [40]. The splice losses for the fibers shown in Fig. 2 are shown in Table 1, along with a summary of the fiber properties. Four commercially available types of single mode fiber are shown and include SMF28, 980HP, UHNA1, UHNA4 (Nufern), the core diameter (CD) and mode field diameter (MFD) are also shown. All calculations were performed at a wavelength of 1550 nm. Note that random polarization in the single mode fiber has been assumed and thus the values in Table 1 assume the total coupling from unpolarized light in the single mode fiber into both polarizations of the fundamental mode of the EC-MOF.

Table 1. Splice loss from SMF into EC-MOF

EC-MOF Description	D-shaped	Offset	Wedged	Small-core
Figure	2(a)	2(b)	2(c)	2(d)
Exposed-core fiber characteristics (μm)				
Outer diameter	200	200	160	200
Core diameter	12.5	9.3	7.5	2.7
Wedge angle (°)	113	158	50	33
MFD[a] (polarization 1)	8.62	6.75	5.18	2.19
MFD[a] (polarization 2)	8.26	6.56	5.07	2.72
Calculated splice loss for SMF to EC-MOF (dB)				
SMF28[b] (MFD = 10.3 μm) (CD = 9.2 μm)	0.49	1.22	2.48	8.28
980HP[b] (MFD = 6.19 μm) (CD = 3.6 μm)	0.55	0.44	0.70	4.07
UHNA1[b] (MFD = 4.51 μm) (CD = 2.5 μm)	1.18	0.66	0.45	2.33
UHNA4[b] (MFD = 3.48 μm) (CD = 2.2 μm)	2.27	1.32	0.65	1.27

[a]Numerically calculated value.
[b]Mode field diameter, core diameter, and refractive index data from: http://www.nufern.com/

It can be seen from Table 1 that the choice of single mode fiber can be used to optimize the splice loss, with values below 0.5 dB being possible for all fiber designs, except for the smallest core (2.7 μm) fiber considered here, where the minimum splice loss is 1.27 dB. If smaller splice losses are required in practice, then intermediate fibers or tapers would need to

be introduced. These results serve as a useful guide for single mode fiber selection, noting that experimentally other factors become significant, most notably structural deformation of the EC-MOF upon heating, and alignment tolerances of the splicer.

2.4 Splicing to conventional single mode fiber: experimental

It was previously shown that the 12.5 µm exposed-core fiber can be spliced to conventional single mode fiber (SMF28e), with a loss as low as 3 dB [40]. In this work we have concentrated our efforts on splicing to the wedged (7.5 µm core) EC-MOF using an arc splicer (Fujikura FSM-100P), motivated by the success in writing Bragg gratings into this fiber (see Sec. 3).

A number of techniques have been presented for optimizing splicing to MOFs, including reducing arc current, offsetting the arc position, and using a tack-sweep-pulse technique [46-48]. In this work we have spliced EC-MOF to SMF with only a small deviation from standard SMF splicing by optimizing the arc current, arc time, and overlap (the distance the two fibers are pushed together). The transmitted power obtained from the EC-MOF after splicing is shown in Fig. 3 relative to the transmitted power when butt-coupling at a gap of 5 µm. The results show that the splice can be optimized by decreasing the arc current while increasing the arc time. Transmission consistently better than the butt-coupled power was found for a current of 4.0 mA below the standard SMF setting, for a duration of 3.0 s (standard is 2.0 s). The results of Fig. 3 also show that an overlap of 2 µm below the standard overlap (10 µm) provides optimal splicing. These results are consistent with trying to minimize damage to the structured fiber. In future, further refinements could be made by further decreasing arc current and increasing arc discharge time. However, the optimized settings found here have proven to provide sufficient coupling for Bragg grating sensor measurements while still being physically robust enough for handling within a laboratory setting.

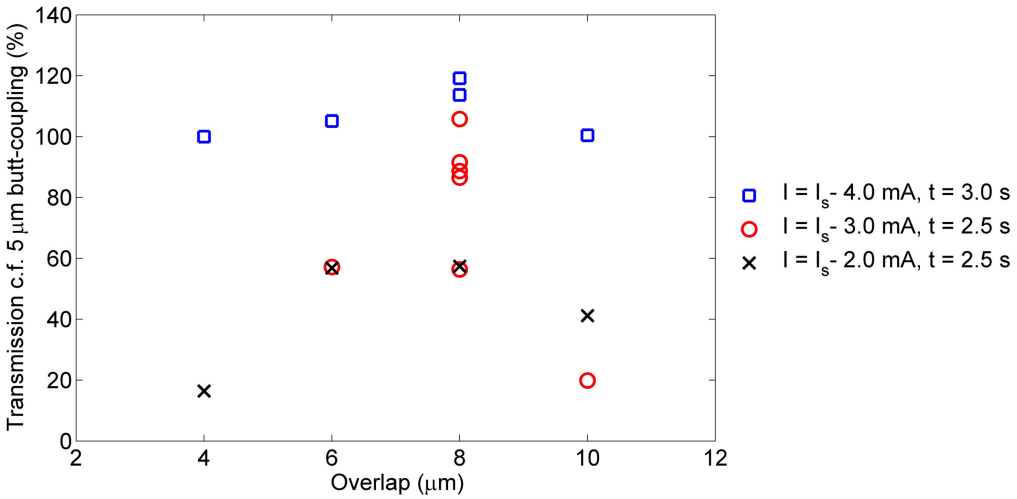

Fig. 3. Transmitted power through 7.5 µm core diameter EC-MOF spliced to 980HP single mode fiber. Power is relative to butt-coupled transmission with a 5 µm offset. I_s is the standard current used by the arc splicer after calibration, approximately 16.5 mA.

The splicing parameters determined in Fig. 3 are quite specific for the particular geometry of the microstructured fiber, the wedged (7.5 µm core) fiber in this case. For example, when splicing to the small-core (2.7 µm) EC-MOF is it much more likely that the fiber structure is damaged, particularly the fine struts. The best splice loss achieved for the small-core EC-MOF was approximately 16.5 dB (settings were: $I = I_s - 3.0$ mA, t = 2.0 s, overlap = 5 µm). For the offset (9.3 µm) core it was found to be difficult to produce a flat cleave using

traditional crack cleaving approaches, particularly near the core region. In future this might be solved by utilizing laser cleaving techniques [49], but is beyond the scope of this study.

3. Longitudinal structure: fiber Bragg gratings

In previous work Bragg gratings were written into the D-shaped (12.5 μm core) EC-MOF [Fig. 1(a)] [40]. Briefly, the gratings were written by focusing a 200 nJ, 200 Hz, 800 nm femtosecond laser (Hurricane Ti:sapphire) pulses using a 50X long working distance microscope objective while translating the fiber along its axis to yield 20 mm long, 1060 nm pitch second order Bragg gratings at 1550 nm.

Writing such structures into EC-MOFs that have an open and accessible core, such as the D-shaped and Offset geometries [Figs. 2(a) and 2(b)], is readily achieved as the focused beam is not obstructed by material. Of particular interest here is the ability to write gratings into exposed-core fiber structures that pose obstructions to the focused femto-second laser beam. For the wedged (7.5 μm core) fiber, which has a wedge angle of 50^{o}, it was found that a femto-second laser pulse energy of 250 nJ was required in order to produce damage spots on the core. This level of obstruction from the fiber geometry does not have a significant impact on the focal point of the femtosecond laser, as shown by the grating produced in Figs. 4(a) and 4(b). Note that the settings used for this grating writing were the same as used for the D-shaped fiber, except that the pulse frequency was reduced from 200 Hz to 100 Hz in order to reduce the speed of the translation stage and improve stability. The length of the Bragg gratings were also varied, between 1 to 20 mm, with longer lengths being required for larger core diameter fibers due to the reduced overlap between the femtosecond laser ablation features and the propagating mode.

The small-core (2.7 μm) fiber with a wedge angle of 33^{o} required a pulse energy of 440 nJ before any ablation occurred. Unfortunately, the ablation occurred at the thin struts holding the core (approximately 1 μm thick) rather than on the surface of the core, as shown in Fig. 4(c). Thus, laser ablation gratings could not be formed on this fiber without significant damage to the fiber structure. For this reason the sensing results that follow have primarily utilized the 7.5 μm core fiber. Gratings were also written into the offset (9.2 μm core) fiber. However, the difficulty found in cleaving and splicing the fiber meant that it could not be used for liquid-based experiments.

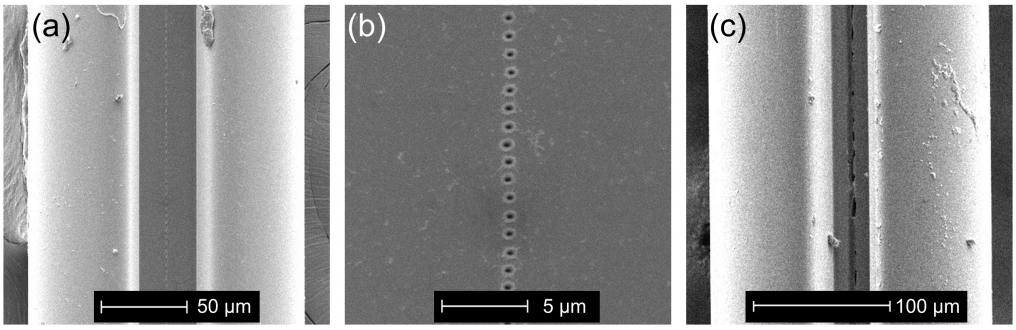

Fig. 4. (a) Femtosecond laser written Bragg gratings in the wedged (7.5 μm core) fiber, written directly on its core. (b) Magnified image of (a). Damage caused on the core of the small core (2.7 μm core) fiber, which results from aberrations to the femtosecond laser beam due to the narrow fiber geometry in combination with the thin struts that support the fiber core.

4. Sensitivity of FBGs to bulk refractive index

The fibers in Figs. 2(a), 2(c), and 2(d) have been characterized for their refractive index sensing performance. These fibers were first spliced to conventional single mode fiber (see Sec. 2.4 and [40]) and the Bragg reflections measured using an Optical Sensor Interrogator (OSI, National Instruments PXIe-4844). In all measurements where liquids were measured,

the far end of the fiber was sealed using the arc splicer to prevent liquid ingress into the MOF holes. The spliced EC-MOF fibers were immersed into refractive index solutions by vertically holding the fibers and inserting into sealed Pasteur pipettes containing isopropanol in water solutions, with the refractive index calculated based on measurements performed by Chu *et al.* [50]. The reflection spectra contains multiple peaks due to higher order modes, however, the narrowest and strongest peak is generally the longest wavelength peak, which corresponds to coupling from the forward to the backward propagating fundamental mode. The spectra obtained for the fundamental mode reflection of the wedged (7.5 μm core) fiber are shown in Fig. 5. As expected, the Bragg wavelength increases as the external refractive index is increased.

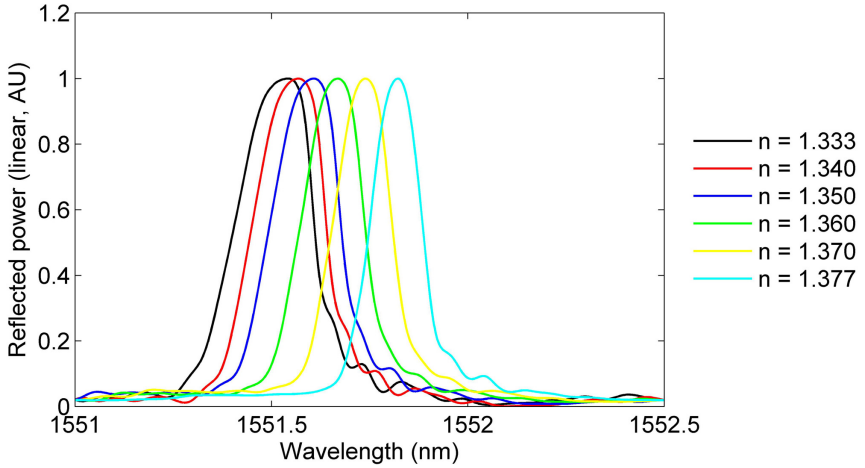

Fig. 5. The reflected Bragg grating spectra when the EC-MOF with a core diameter of 7.5 μm [Fig. 2(c)] was immersed in different refractive index liquids. The refractive index was varied by dissolving isopropanol in water. Only the longest wavelength is shown, which corresponds to the fundamental mode.

To compare the sensitivity of the various core diameters, both theoretically and experimentally, the fundamental mode Bragg wavelengths for refractive index solutions ranging from 1.0 (air) to 1.4 are shown in Fig. 6. The theoretical curves were generated by importing SEM images into COMSOL v3.4, as was done for the coupling efficiency, and varying the refractive index of the exposed region of the fiber. The Bragg grating pitch (Λ) was varied slightly in order to achieve the best fit with experiment (Λ = 1080 nm + (a) 1.03 nm, (b) 1.22 nm, (c) 1.00 nm). The experimental points for Fig. 6(a) were from [40] and those for Fig. 6(b) were obtained from Fig. 5. For the small-core (2.7 μm) EC-MOF a 2 mm long grating was used. In this case a particularly weak grating (< 1 dB) formed, due to a combination of the damage during the grating writing, high splice loss, and a high background reflection that resulted from the splice. Thus, the experimental results in Fig. 6(c) consist of only two data points, which were in air (n = 1.0) and water (n = 1.33). Attempts to measure the grating position for higher index solutions were unsuccessful, indicating a substantial challenge in using such small core fibers for measuring refractive index solutions using a Bragg grating approach.

The wedged (7.5 μm core) fiber grating shifted by approximately 0.28 nm over the refractive index range from 1.333 (water) to 1.377 (isopropanol). This corresponds to an average sensitivity over this range of 6.4 nm/RIU. This is a significant improvement compared to a shift of only 0.076 nm (1.7 nm/RIU) that was measured over the same range for the D-shaped (12.5 μm core) fiber [40]. Despite difficulties in coupling, the sensitivity of the

small-core (2.7 μm) fiber, as shown by the numerically calculated curve and two closely fitting experimental points in Fig. 6(c), is much higher at 101 nm/RIU over the same range.

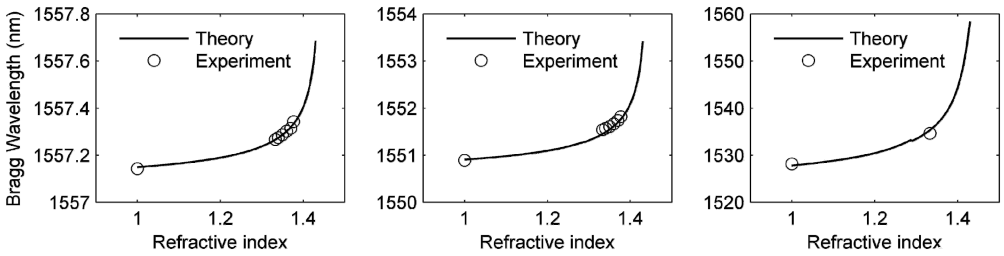

Fig. 6. Refractive index sensitivity curves for the (a) D-shaped (12.5 μm core), (b) wedged (7.5 μm core), and (c) small-core (2.7 μm) EC-MOFs, both theoretical (lines) and experimental (circles). The grating lengths used were (a) 20 mm, (b) 10 mm, and (c) 2 mm.

5. Characterizing the polyelectrolyte layer deposition

For biological sensing with silica fibers it is often desirable to modify the functional groups present on the glass surface in order to optimize binding of specific biological material. One versatile technique is to coat the surface with polyelectrolytes [13, 22, 51, 52]. These coatings are formed by stacking alternating charged layers of electrostatic polymers and can provide a host of functional groups on the surface such as amine or carboxylic acid groups. By using a technique that is capable of measuring refractive index on the surface it is possible not only to measure the layers being deposited but to also use this as a calibration curve for subsequent biological binding. Thus, measuring polyelectrolyte layer deposition is an important first step in developing this class of biosensor. Here we have coated the wedged (7.5 μm) core EC-MOF with two bi-layers of polyelectrolytes to demonstrate the potential use of the FBG written on EC-MOF for biosensing applications.

In this experiment the optical sensor interrogator was connected to an in-line polarizer and then polarization maintaining fiber (Nufern, PM980-XP). The polarization maintaining fiber was then spliced to the EC-MOF using the optimized conditions from Sec. 2.4. Fixing the polarization in this manner prevents the reflected spectra from being modified if the single mode fiber cable is moved during the course of the experiment. The Bragg grating used was 10 mm long with a second order reflection at approximately 1550 nm while the total length of the EC-MOF was 100 mm long with the grating in the center. The entire length of the EC-MOF was then inserted into a flow cell, which consisted of a silica capillary (approx. 1 mm inner diameter (ID)) with an inlet capillary (150 μm ID) that was connected to a syringe pump (Nanojet) and another outlet capillary (150 μm ID). In this experiment the syringe pump was set at 0.1 mL/min for all steps. Prior to polyelectrolyte deposition the flow cell, containing the EC-MOF, was rinsed with water (Millipore) for 50 minutes. Solutions of 2 mg/ml Poly(sodium styrene sulphonate) (PSS) and poly(allylamine hydrochloride) (PAH) in 1 M NaCl were then passed through the flow cell for 20 minutes alternatively, with a 30 minute minimum water rinsing time between each step.

The shift in the Bragg grating reflection associated with each polyelectrolyte layer is shown in Fig. 7(a). These values correspond to the measurements recorded once per minute during the last 10 minutes of the rinsing phase, after the signal had reached equilibrium. The shift was recorded in the rinsing phase rather than the coating phase as it is important to measure in the same refractive index solution (water in this case). The error bars in Fig. 7(a) refer to the standard deviation of the 10 spectra recorded over the 10 minutes of measurement. The shift in Bragg reflection was determined by calculating the weighted mean of the longest reflection peak (the fundamental mode reflection) as indicated in Fig. 7(b). The weighted mean of the Bragg reflection, λ_w, was calculated using Eq. (2).

$$\lambda_w = \frac{\int \lambda I_B(\lambda) d\lambda}{\int I_B(\lambda) d\lambda} \tag{2}$$

In Eq. (2), the integrals were calculated over the wavelength range from λ = 1551.4 nm to λ = 1552.0 nm and I_B is the linear intensity of the Bragg reflection.

This allows the wavelength resolution to be improved over the 4 pm values provided by the instrumentation. The positive shift observed in Fig. 7(a) is consistent with polyelectrolyte layer deposition, which increases the refractive index on the surface of glass. Thus, we have demonstrated that the Bragg grating sensor formed from the 7.5 µm core EC-MOF is sufficiently sensitive to characterize the growth of polyelectrolyte layer deposition. This serves as a useful step towards turning an EC-MOF into a biological sensor as it is both sensitive and has the functional groups required (in this case amine groups) to allow for biological binding.

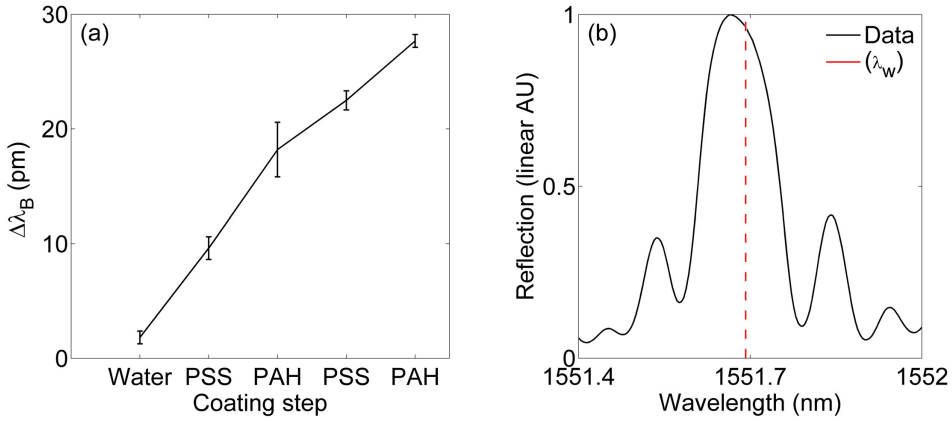

Fig. 7. (a) Shift in the Bragg wavelength as each polyelectrolyte coating is added. (b) Example spectra indicating the position of the weighted mean (λ_w), which was used to determine the values in (a).

6. Discussion and conclusions

We have demonstrated experimentally that reducing the core diameter of exposed-core microstructured optical fibers can improve the sensitivity for refractive index sensing using Bragg gratings, which is due to an increase in the portion of the guided mode that propagates externally to the optical fiber glass. By reducing the core diameter to 7.5 µm the experimentally measured sensitivity is increased to 6.4 nm/RIU over the refractive index range of 1.333 to 1.377, compared to the previously demonstrated result of 1.7 nm/RIU using a 12.5 µm core fiber. Theoretical modelling based on SEM images of fabricated fibers predict that sensitivities as high as 101 nm/RIU should be achievable using a 2.7 µm core fiber. While the sensitivity is unlikely to outperform techniques such as surface plasmon resonance, the capability of Bragg grating sensors to be multiplexed and operate in reflection mode makes them particularly attractive for performing label-free immunoassays in *in-vivo* biosensing applications.

The increase in sensitivity of smaller core fibers must then be traded against the practicality of these fibers. In particular, the ability to cleave and splice the fibers to conventional single mode fiber is critical in accessing the viability of the fiber to be used for sensing. The wedged (7.5 µm core) fiber was found to splice readily to SMF, and optimized settings have allowed for high transmission efficiencies. On the other hand, fibers that have an offset, or non-central, core or fibers with small cores were found to be challenging to splice with high efficiency or repeatability, despite low theoretical losses. This is likely attributed to

the difficulty in obtaining a flat cleave at the core and struts, and thus advanced techniques such as laser cleaving may be required.

The next critical factor to consider is the ability to write gratings onto the core of these fibers. Open structures with unimpeded access to the core have been found to be well suited to writing femtosecond laser ablated gratings. It is also possible to write gratings if the exposed section of the fiber is formed from a narrower slot, up to a point where the wedge is significantly obstructing the beam. In future, alternative techniques such as oil immersion or choice of a different focusing lens could be used to write gratings into narrower features.

Of the fibers considered here, the 7.5 μm exposed-core microstructured optical fiber has been found to be the best compromise between practicality and sensitivity when fabricating a refractive index sensor. In future it would be ideal to fabricate fibers with a similar geometry but with core diameters in the range of 4-5 μm that sit in the region between single-step and two-step preform fabrication using currently available facilities. Such fibers should exhibit improved sensitivity, while still being practical to handle, and thus allow for the direct measurement of biomolecule binding.

Acknowledgments

The authors acknowledge Ben Johnston from Macquarie University for assistance in writing the Bragg gratings and Peter Henry, Heike Ebendorff-Heidepriem, and Erik Schartner from the University of Adelaide for their contribution to the silica fiber fabrication. This work was performed in part at the OptoFab node of the Australian National Fabrication Facility utilizing Commonwealth, and South Australian and New South Wales State Government funding. Stephen Warren-Smith and Linh Nguyen acknowledge the support of an Australian Research Council (ARC) Super Science Fellowship and Tanya Monro acknowledges the support of an ARC Georgina Sweet Laureate Fellowship. This work is supported via the Sensing Technologies for Advanced Reproductive Research (STARR) laboratory, supported by the South Australian State Government via the Premier's Science & Research Fund (PSRF) scheme. The authors acknowledge the Australian Defence Science and Technology Organisation (under the Signatures, Materials and Energy Corporate Enabling Research Program) for support of the suspended and exposed core silica fiber development at The University of Adelaide and funding from the ARC Centre of Excellence in Nanoscale BioPhotonics.